Bioconjugate Chemistry

pubs.acs.org/bc

Article

Rationally Designed ACE2-Derived Peptides Inhibit SARS-CoV-2

Ross C. Larue,* Enming Xing, Adam D. Kenney, Yuexiu Zhang, Jasmine A. Tuazon, Jianrong Li, Jacob S. Yount, Pui-Kai Li, and Amit Sharma*

Cite This: https://dx.doi.org/10.1021/acs.bioconjchem.0c00664

Read Online

ACCESS | Metrics & More | Article Recommendations

ABSTRACT: Severe acute respiratory syndrome coronavirus (SARS-CoV)-2 is a novel and highly pathogenic coronavirus and is the causative agent of the coronavirus disease 2019 (COVID-19). The high morbidity and mortality associated with COVID-19 and the lack of an approved drug or vaccine for SARS-CoV-2 underscores the urgent need for developing effective antiviral therapies. Therapeutics that target essential viral proteins are effective at controlling virus replication and spread. Coronavirus Spike glycoproteins mediate viral entry and fusion with the host cell, and thus are essential for viral replication. To enter host cells, the Spike proteins of SARS-CoV-2 and related coronavirus, SARS-CoV, bind the host angiotensin-converting enzyme 2 (ACE2) receptor through their receptor binding domains (RBDs). Here, we rationally designed a panel of ACE2-derived peptides based on the RBD-ACE2 binding interfaces of SARS-CoV-2 and SARS-CoV. Using SARS-CoV-2 and SARS-CoV Spike-pseudotyped viruses, we found that a subset of peptides inhibits Spike-mediated infection with IC_{50} values in the low millimolar range. We identified two peptides that bound Spike RBD in affinity precipitation assays and inhibited infection with genuine SARS-CoV-2. Moreover, these peptides inhibited the replication of a common cold causing coronavirus, which also uses ACE2 as its entry receptor. Results from the infection experiments and modeling of the peptides with Spike RBD identified a 6-amino-acid (Glu37-Gln42) ACE2 motif that is important for SARS-CoV-2 inhibition. Our work demonstrates the feasibility of inhibiting SARS-CoV-2 with peptide-based inhibitors. These findings will allow for the successful development of engineered peptides and peptidomimetic-based compounds for the treatment of COVID-19.

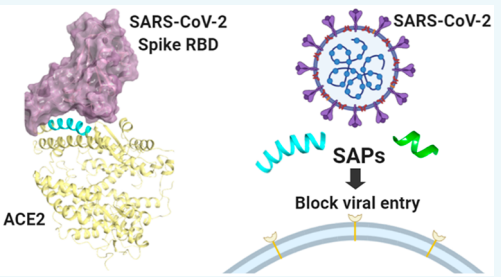

INTRODUCTION

Coronavirus disease 2019 (COVID-19) is an ongoing pandemic that has posed a serious threat to public health and the global economy. The causative agent of COVID-19 is a novel coronavirus, severe acute respiratory syndrome coronavirus (SARS-CoV)-2, which first emerged in late 2019 in Wuhan City, China.[1,2] By March 2020, the World Health Organization had declared COVID-19 a pandemic. The rapid spread of SARS-CoV-2 is attributable to its high reproductive number, community and asymptomatic spread through close contact, and airborne transmission of respiratory droplets and aerosols.[3−5] COVID-19 patients can become critically ill with severe hypoxemia, viral pneumonia, acute respiratory distress syndrome, and gastrointestinal and neurological symptoms.[6−9] To date, there is no approved drug or vaccine for SARS-CoV-2, with the best treatments being supportive care and repurposed drugs.[10,11] A wide array of diverse approaches are urgently needed to rapidly and effectively advance antiviral therapies.

Of the seven coronaviruses known to infect humans, SARS-CoV-2 and two other highly pathogenic coronaviruses, SARS-CoV and Middle East respiratory syndrome coronavirus (MERS-CoV), are the result of zoonotic transmission.[12] Sequence analyses of coronaviruses have revealed that the SARS-CoV-2 genome shares ∼80% identity with SARS-CoV and ∼96% identity with bat coronavirus RaTG13.[1,13] Similar to all coronaviruses, SARS-CoV-2 virions display the characteristic club-shaped projections formed by trimers of viral Spike glycoprotein on their surface.[14] Spike proteins are essential for viral replication as they mediate viral entry into the host cell. During virion morphogenesis, the trimeric Spike protein is cleaved into the S1 and S2 subunits.[15−18] The cleavage event positions the receptor-binding domain (RBD) in the S1 subunits in a receptor-accessible conformation and induces structural changes in the S2 subunits to stabilize its prefusion state.[19−21] SARS-CoV and SARS-CoV-2 RBDs bind to the peptidase domain of human angiotensin-converting enzyme 2 (ACE2), which serves as the viral entry receptor.[18,22] Binding of the RBD to ACE2 triggers another cleavage event of the S2 subunit, which results in formation of the six-helix bundle fusion core necessary for viral−host membrane fusion.[18,23−25]

Received: December 2, 2020
Revised: December 8, 2020

The essential role of Spike protein in receptor binding and viral fusion makes it a prime target for vaccine candidate development and therapeutic interventions.

Seminal SARS-CoV and SARS-CoV-2 structural studies have revealed the overall structures of Spike trimers, detailed atomic level structures of RBD bound to ACE2, and structural intermediates of the Spike-ACE2 interaction events.[19,21,26−31] These structural studies have identified that SARS-CoV and SARS-CoV-2 Spikes bind ACE2 with a nearly identical binding mode—the N-terminal lobe of the ACE2 peptidase domain binds a concave groove on the Spike RBD. Moreover, these studies highlighted that SARS-CoV and SARS-CoV-2 have conserved interactions at the RBD-ACE2 binding interface. For example, 17/20 contacting amino acid residues in ACE2 have conserved interactions with the two RBDs. Likewise, 13/14 contacting residues in the two RBDs are either conserved or have conservatively substituted side chains. Given the significance of the RBD-ACE2 interaction interface for SARS-CoV-2 infection, computational approaches have identified potential inhibitory peptides that could interfere with the interaction of Spike protein with ACE2.[32−35] These theoretical studies have suggested that regions in Spike and select residues in ACE2 could be exploited for competitive inhibition. While potentially promising, the antiviral potential of such peptides has not been experimentally evaluated.

Here, we performed comparative analyses of the SARS-CoV and SARS-CoV-2 RBD-ACE2 interaction interfaces to rationally design a panel of Spike-targeting ACE2-derived peptides (SAPs). A combination of approaches were used to evaluate the inhibitory potential, selective inhibition, and binding affinity of SAPs. Antiviral potential of selected SAPs was validated against two pathogenic human coronaviruses, SARS-CoV-2 and HCoV-NL63, both of which use ACE2 as entry receptors. Importantly, our findings provide a proof-of-principle and demonstrate feasibility of inhibiting SARS-CoV-2 infection by disrupting the Spike-ACE2 interaction interface with peptide-based inhibitors.

RESULTS AND DISCUSSION

Rational Design of ACE2-Derived Peptides. In order to design a panel of small peptide-based inhibitors that can block the interaction of SARS-CoV-2 Spike with the ACE2 receptor, we utilized a combination of existing structural and biochemical data, and known amino acid interactions necessary for binding of SARS-CoV and SARS-CoV-2 Spike proteins to ACE2. This included (1) crystal structures of ACE2 bound to SARS-CoV and SARS-CoV-2 Spike receptor binding domains (RBDs);[19,30,31] (2) cryoEM structures of ACE2 in complex with trimeric SARS-CoV Spike and RBD or S1 subunit of SARS-CoV-2 Spike;[21,26,29] and (3) biochemical binding data of the ACE2-interacting motif with the SARS-CoV and SARS-CoV-2 Spikes.[27,30] In particular, we focused on the Spike-ACE2 interaction interface, as it offers a prime target for competitive inhibition of viral entry. Structural and biochemical analyses have shown that SARS-CoV and SARS-CoV-2 RBDs bind ACE2 with nearly identical binding modes and with similar low nanomolar binding affinities. The α1 helix of ACE2, which is cradled in a concave groove formed by the β5 and β6 sheets of the RBD, provides the most contacts with the two RBDs (ACE2 residues Gln24, Thr27, Phe28, Lys31, His34, Glu37, Asp38, Tyr41, and Gln42). Additional contacts from ACE2 are provided by α3 helix (ACE2 residues Leu79, Met82, Tyr83 for the two RBDs), a short loop between α10 and α11 helices (ACE2 residues Gln325 and Glu329 for SARS-CoV RBD and Asn330 for both RBDs), β-hairpin flanking α11 helix (ACE2 residue Lys353 for both RBDs), and α11 helix (ACE2 residues Gly354, Asp355, and Arg357 for both RBDs). Conversely, 14 residues (402, 426, 436, 440, 442, 472, 473, 475, 479, 484, 486, 487, 488, and 491) in the two RBDs provide contacts with ACE2. These RBD residues form a network of hydrogen bonds, salt bridges, and van der Waals contacts with ACE2 residues. Based on these insights, we designed six Spike-targeting ACE2-derived peptides (SAPs)—four derived from α1, one derived from α3, and one derived from α11 helix of ACE2 (Table 1). The SAPs were designed using the following criteria: (1) they contain at least three residues predicted to interact with RBDs based on structural data (Table 1, highlighted in bold); (2) they are not highly disordered or unresolved in the crystal structures (such as ACE2 residues 1−18); and (3) the length is more than 6 and less than 30 amino acids, making them amenable for synthesis.

Table 1. Spike-Targeting ACE2-Derived Peptides (SAPs) Used in This Study[a]

Peptide	Amino Acid Sequence	Location
SAP1	27-**TF**L**DK**FN**HE**A**EDLFYQ**-42	Helix-1
SAP2	37-**EDLFYQ**S**SL**-45	Helix-1
SAP3	79-LAQ**MY**PL-85	Helix-3
SAP4	352-G**KGDFR**IL-359	Helix-11
SAP5	24-Q**AKTF**L**DK**FN**HE**A-36	Helix-1
SAP6	37-**EDLFYQ**-42	Helix-1

[a]Amino acid sequence with the residue number of the first and last amino acid in the sequence is indicated. The essential EDLFYQ motif is indicated in red. The SARS-CoV and SARS-CoV-2 contacting residues are indicated in bold.

SAPs Inhibit SARS-CoV-2 Spike-Pseudotyped Lentivirus Infection. We evaluated the antiviral potencies of SAPs against lentiviral vectors pseudotyped with SARS-CoV-2 Spike glycoprotein. Lentiviral cores pseudotyped with viral surface glycoproteins offer an alternative to highly pathogenic viruses that require biosafety level 3 (BSL3) or BSL4 facilities.[36] Importantly, pseudotyped viruses can be utilized at BSL2 and are ideal for studies pertaining to viral entry and screening of therapeutic agents that target viral entry, such as the peptides in this study. *Luciferase*-encoding lentiviruses pseudotyped with SARS-CoV-2 Spike were incubated with test peptides to allow binding to the vector particle-associated Spike prior to infection of HEK293T-ACE2 cells. Luciferase production was measured 48 h post-infection. A titration curve for each peptide was generated for determining its inhibitory concentration (IC_{50}). Of the six SAPs tested, SAP1, SAP2, and SAP6 inhibited SARS-CoV-2 Spike-mediated virus infection with an IC_{50} value of 2.39 ± 0.20, 3.72 ± 0.37, and 1.90 ± 0.14 mM, respectively (Figure 1). In contrast, 50% inhibition of Spike-mediated virus infection was not achieved with SAP3, SAP4, or SAP5 even at 7.5 mM, the highest concentration tested. Thus, three of the six SAPs inhibit SARS-CoV-2 Spike-mediated virus infection with IC_{50} values in the low millimolar range.

Despite the fact that the genomes of SARS-CoV and SARS-CoV-2 share ∼80% sequence identity and most of the sequence variation is within the Spike open reading frame,[1] the overall structure and ACE2-binding mode of their Spike RBDs are nearly identical. Moreover, the majority of amino acid residues in the SARS-CoV and SARS-CoV-2 RBDs that

https://dx.doi.org/10.1021/acs.bioconjchem.0c00664
Bioconjugate Chem. XXXX, XXX, XXX−XXX

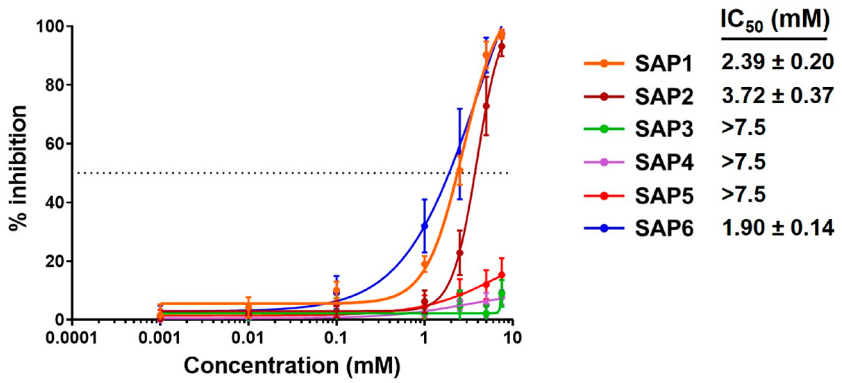

Figure 1. Dose-dependent inhibition of SARS-CoV-2 Spike-pseudotyped lentivirus infection by SAPs. Dose response curves of the indicated SAPs generated by plotting the percent viral inhibition (*y*-axis) against the log transformation of SAP concentration (mM, *x*-axis). Each data point represents the average of three independent experiments, performed in duplicate. Error bars represent standard deviations. The dotted gray line indicates 50% viral inhibition used to determine the IC_{50} value. Computed IC_{50} values for the indicated SAPs from three independent experiments ± standard deviations are shown.

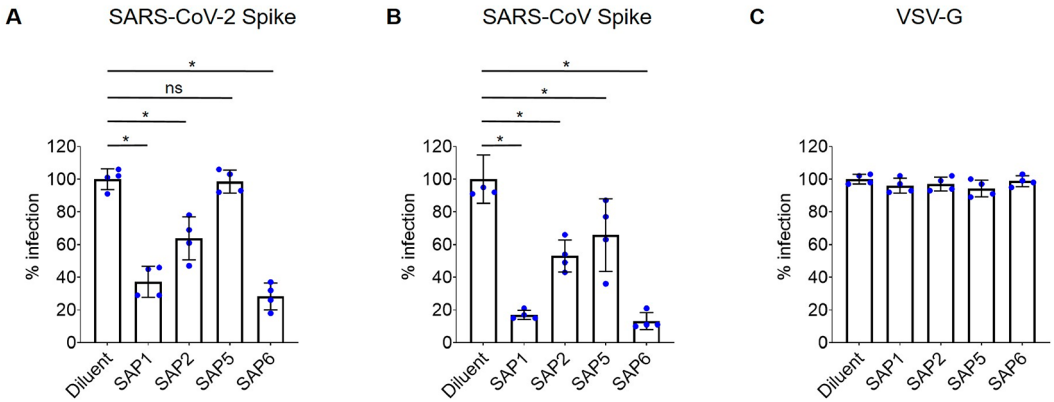

Figure 2. Inhibition of Spike- and VSV-G-pseudotyped lentivirus infection by SAPs. *Luciferase*-encoding lentiviruses pseudotyped with indicated viral glycoprotein were incubated with 3 mM of indicated SAP or diluent control for 1 h prior to infection of 293T-ACE2 cells. Infection was measured as relative luciferase expression 48 h post-infection. The luciferase signal obtained for the diluent control was set to 100%. Graphs indicate the percentage of infected cells normalized to the diluent control for lentiviruses pseudotyped with (A) SARS-CoV-2 Spike, (B) SARS-CoV Spike, or (C) VSV-G. Bars represent averages from four independent experiments, performed in duplicate, with means from individual experiments shown as circles. Error bars represent standard deviations. Percent infections were compared to the diluent control using one-way analysis of variance (ANOVA) followed by Dunnett's multiple comparisons test. * $p < 0.05$; ns, not significant.

are essential for binding ACE2 either are identical or have conserved side chains.[29−31] Thus, we sought to determine whether SAPs that inhibit SARS-CoV-2 Spike-mediated virus infection are also able to inhibit infection mediated by SARS-CoV Spike. For this, SAPs with positive inhibitory profiles from Figure 1 were evaluated for their ability to inhibit infection of SARS-CoV Spike- and SARS-CoV-2 Spike-pseudotyped viruses at 3 mM dose, which is within the IC_{50} range for the test peptides (Figure 1). As specificity control, antiviral activity of SAPs was also measured against lentiviruses pseudotyped with vesicular stomatitis virus Glycoprotein (VSV-G), which utilizes low-density lipoprotein receptor, LDL-R, for viral entry.[37] In comparison to the diluent control, SAP1, SAP2, and SAP6 treatment resulted in ∼1.6−3.5-fold reduction in SARS-CoV-2 Spike-mediated infection (Figure 2A) and ∼1.9−7.5-fold reduction in SARS-CoV Spike-mediated infection (Figure 2B). Consistent with the results in Figure 1, SAP5 treatment had no significant effect on SARS-CoV-2 Spike-mediated infection, but resulted in ∼1.5-fold reduction in SARS-CoV Spike-mediated infection. None of the SAPs affected VSV-G-mediated virus infection demonstrating their specificity for inhibiting Spike-mediated viral entry (Figure 2C). The slightly higher potency of SAP1, SAP5, and SAP6 against SARS-CoV Spike-mediated infection compared to SARS-CoV-2 Spike-mediated infection could be attributable to subtle differences in the SARS-CoV and SARS-CoV-2 RBD-ACE2 interaction interfaces.[29−31] Importantly, these results highlight the fact that minor differences in the number of contact residues and their interactions at the RBD-ACE2 interface could be exploitable for structure-based rational design of viral-specific inhibitors.

Binding Affinities of SAPs to SARS-CoV-2 Spike RBD. Recent studies using biochemical and biophysical methods have demonstrated that the RBD within the S1 subunit of SARS-CoV-2 Spike is responsible for binding ACE2 with high affinity.[27,30] Thus, we employed affinity precipitation assays to determine the binding affinities of SAPs with positive inhibitory profiles to recombinantly expressed and purified Spike RBD. A titration curve for each FITC-labeled peptide was generated for determining its binding affinity to His-tagged Spike RBD (Figure 3A and B). Of the four SAPs tested, SAP1 displayed the highest binding affinity (K_d = 0.53 ± 0.01 mM), whereas SAP5 did not display any detectable binding *in vitro* (Figure 3B). SAP6, which contains the overlapping region in

https://dx.doi.org/10.1021/acs.bioconjchem.0c00664
Bioconjugate Chem. XXXX, XXX, XXX−XXX

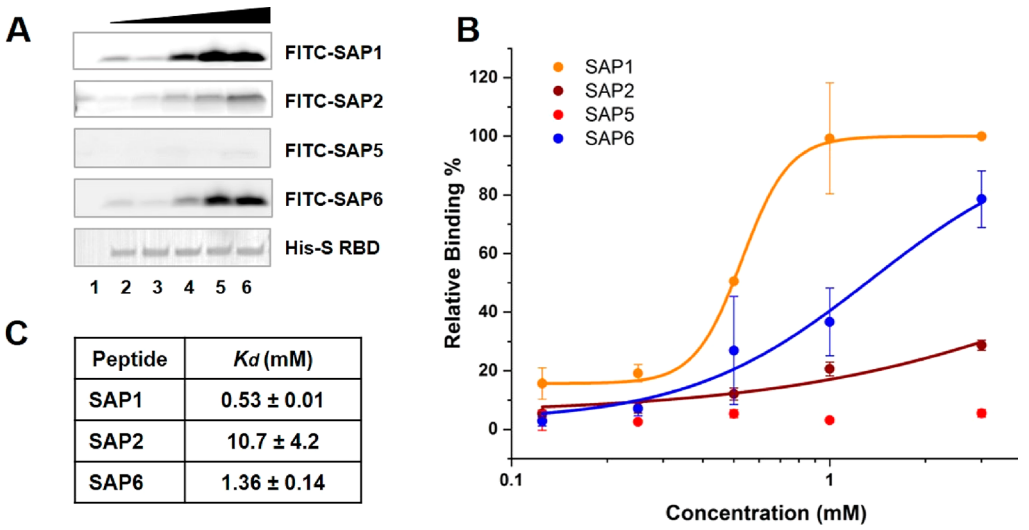

C

Peptide	*Kd* (mM)
SAP1	0.53 ± 0.01
SAP2	10.7 ± 4.2
SAP6	1.36 ± 0.14

Figure 3. Binding of SAPs to SARS-CoV-2 Spike. Affinity precipitation of His-tagged SARS-CoV-2 Spike RBD (indicated "His-S RBD") with FITC-SAPs. (A) Representative SDS-PAGE gels of affinity precipitation of His-S RBD with increasing concentrations of indicated FITC-SAP (lanes 2−8: 0.125, 0.25, 0.5, 1, and 3 mM FITC-SAP). Lane 1 indicates control precipitation of 3 mM FITC-SAP without His-S RBD. FITC-labeled bands were detected at 488 nm fluorescence and His-S RBD was visualized with Coomassie staining. (B) Graphical representation of fluorescence intensities from (A) of indicated FITC-SAP bound to His-S RBD. Each data point represents the average of three independent experiments. Error bars represent standard deviations. Data were fit to the Hill equation to determine the apparent K_d of binding. (C) Calculated binding K_d from three independent experiments ± standard deviations.

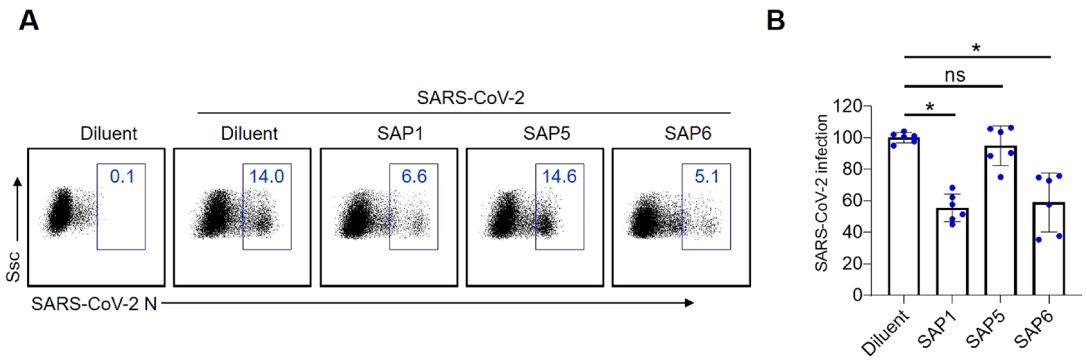

Figure 4. Inhibition of SARS-CoV-2 infection by SAPs. SARS-CoV-2 was incubated with 3 mM of indicated SAP or diluent control for 1 h prior to infection of 293T-ACE2-GFP cells. Infection was measured by flow cytometry as the percentage of cells positive for SARS-CoV-2 nucleocapsid (N) protein 24 h post-infection. (A) Representative flow cytometry plots indicating percent infection. (B) Graph indicates the percentage of infected cells normalized to the diluent control, which was set to 100%. Bars represent averages from two independent experiments, performed in triplicate, with individual data points shown as circles. Error bars represent standard deviations. Percent infections were compared to the diluent control using one-way analysis of variance (ANOVA) followed by Dunnett's multiple comparisons test. * $p < 0.05$; ns, not significant.

SAP1 and SAP2 (Table 1), displayed binding affinity similar to that of SAP1 (Figure 3C, SAP6 K_d of 1.36 ± 0.14 mM vs SAP1 K_d = 0.53 ± 0.01 mM). SAP2 displayed lower binding (K_d = 10.7 ± 4.2 mM) possibly attributable to the presence of two consecutive serine residues in the peptide, which could affect its flexibility. Thus, our results suggest that SAP6 contains the minimal residues needed for binding RBD, and additional residues in SAP1 can slightly improve the binding affinity. Moreover, we found that the *in vitro* binding affinities of SAPs track closely with their antiviral IC_{50} values (Figures 1 and 3).

SAP1 and SAP6 Inhibit SARS-CoV-2 Infection. We next sought to determine whether SAPs that bind RBD with high affinity and display positive inhibitory profiles against pseudotyped viruses are also able to inhibit the infection of genuine SARS-CoV-2. To this end, SAP1, SAP5, and SAP6 were evaluated for their ability to inhibit infection of SARS-CoV-2. Viruses was incubated with 3 mM of test peptide or diluent control to allow binding to the virion-associated Spike prior to infection of HEK293T-ACE2-GFP cells. Percent infection was measured by intracellular staining of SARS-CoV-2 N protein and flow cytometry 24 h post-infection. In comparison to the diluent control, SAP1 and SAP6 treatment resulted in ∼2-fold reduction in SARS-CoV-2 infection (Figure 4A and B). In contrast, SAP5, which does not bind RBD and does not inhibit SARS-CoV-2 Spike-pseudotyped lentiviruses, had no significant effect on virus infection. Based on the findings that SAP1 and SAP6 have comparable IC_{50} values (Figure 1), bind RBD with similar affinity (Figure 3C), and inhibit SARS-CoV-2 infection to similar levels (Figure 4B), we conclude that SAP6 contains the minimal necessary residues for inhibition of SARS-CoV-2.

SAP1 and SAP6 Inhibit HCoV-NL63 Infection. In addition to the three highly pathogenic coronaviruses known to infect humans, four low pathogenicity coronaviruses (HCoV-229E, HCoV-OC43, HCoV-HKU1, HCoV-NL63) are endemic in humans and cause common cold and upper

https://dx.doi.org/10.1021/acs.bioconjchem.0c00664
Bioconjugate Chem. XXXX, XXX, XXX−XXX

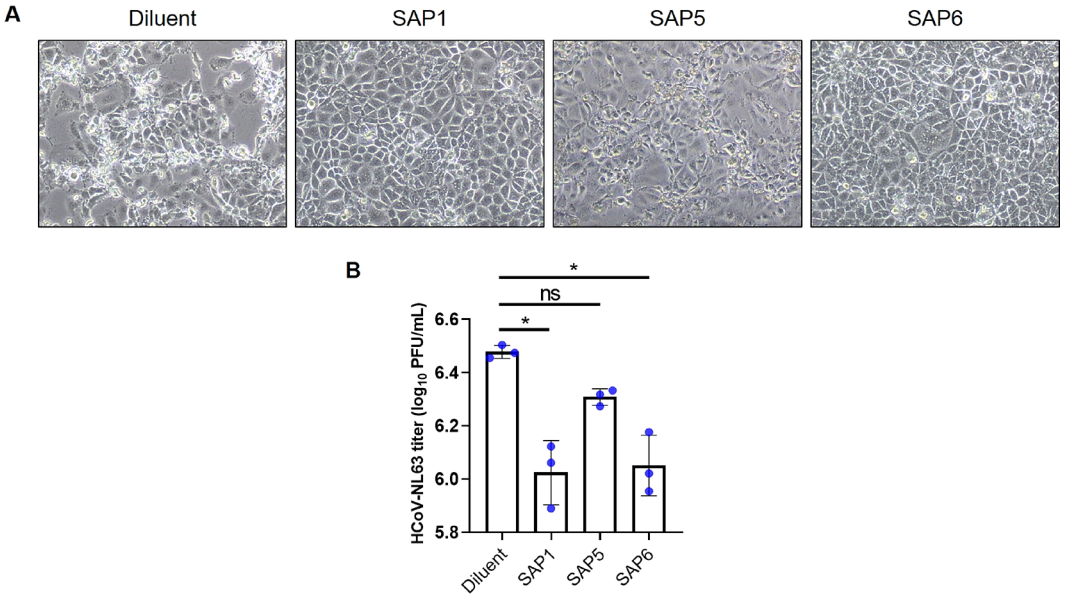

Figure 5. Inhibition of HCoV-NL63 infection by SAPs. HCoV-NL63 was incubated with 3 mM of indicated SAP or diluent control for 1 h prior to infection of LLC-MK2 cells. Cytopathic effects and virus titers in the supernatants were analyzed at 72 h post-infection. (A) Representative bright field microscope images showing cytopathic effects. (B) Graph indicates virus titers in supernatants from LLC-MK2 cells. Bars represent averages from triplicate infections with individual data points shown as circles. Error bars represent standard deviations. Virus titers were compared to the diluent control using one-way analysis of variance (ANOVA) followed by Dunnett's multiple comparisons test. * $p < 0.05$; ns, not significant.

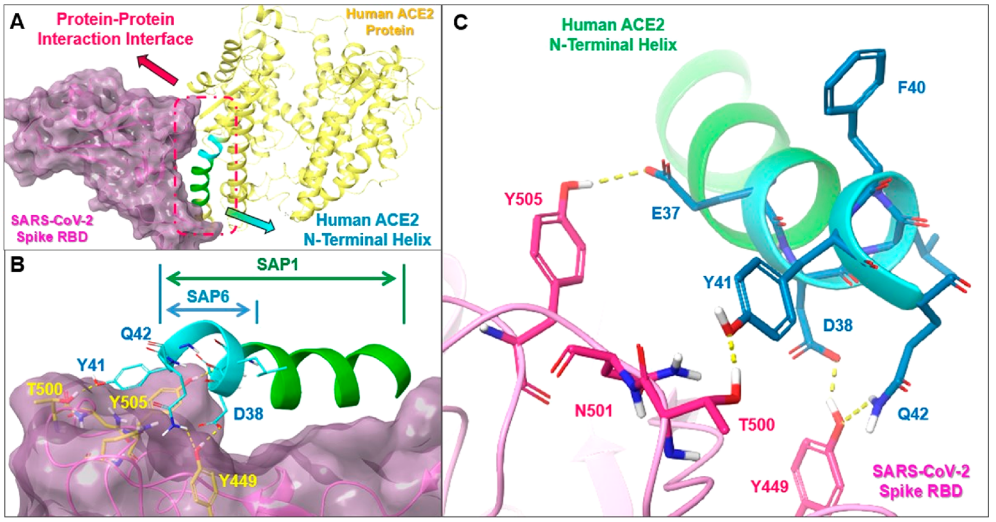

Figure 6. Graphical illustration of SARS-CoV-2 Spike and SAP6 interaction interface. (A) Overall view of SARS-CoV-2 Spike RBD and human ACE2 interaction mode. The N-terminal helix of human ACE2 is located at the central interface. (B) Relative location of SAP6 (light blue) and SAP1 (green and light blue). (C) H-bond interaction network between SAP6 and SARS-CoV-2 Spike RBD. The Y41, Q42, D38, and E37 of SAP6 peptide are involved in H-bond interactions with T500, Y449, N501, and Y505 of SARS-CoV-2 Spike RBD. Corresponding crystal structure: PDB Code: 6M0J. http://www.rcsb.org/structure/6M0J.

and lower respiratory tract infections.[38−40] Of the four endemic human coronaviruses, only HCoV-NL63 uses ACE2 as an entry receptor.[41] Similar to SARS-CoV and SARS-CoV-2, the S1 subunit of HCoV-NL63 Spike binds ACE2 to mediate viral entry.[42] Thus, we sought to determine whether SAP1 and SAP6, which inhibit SARS-CoV-2 infection, could also inhibit HCoV-NL63 infection. Viruses were incubated with 3 mM of test peptide or diluent control to allow binding to the virion-associated Spike prior to infection of LLC-MK2 cells. Virus-induced cytopathic effects (CPEs) and virus titers in the supernatants were measured 72 h post-infection. Severe CPEs were observed in cells that were infected with viruses treated with diluent control or SAP5 indicating robust viral infection (Figure 5A). In contrast, reduced CPEs were observed in cells infected with SAP1- or SAP6-treated viruses indicating reduced viral infection. Moreover, in comparison to the diluent control, SAP1 and SAP6 treatment resulted in ∼3-fold reduced HCoV-NL63 titers (Figure 5B). In contrast, SAP5 treatment did not result in significant reduction of viral titers. Taken together, our results demonstrate that SAP1 and SAP6 inhibit infection of SARS-CoV-2 and HCoV-NL63, both of which utilize ACE2 as entry receptor.

Structural Modeling of SAP1 and SAP6 with SARS-CoV-2 Spike. The findings from our infectivity assays suggest

https://dx.doi.org/10.1021/acs.bioconjchem.0c00664
Bioconjugate Chem. XXXX, XXX, XXX−XXX

that SAP1 and SAP6, and to a lesser degree SAP2, block the interaction of SARS-CoV-2 Spike with ACE2. We found that both SAP1 and SAP6 inhibit SARS-CoV-2 infection to similar levels. Since SAP6 contains the minimal conserved short EDLFYQ motif present in SAP1 and SAP2, we conclude that it is the minimal essential motif important for inhibition of SARS-CoV-2. The cocrystal structure of SARS-CoV-2 Spike RBD and human ACE2 has been recently solved and available through the Protein Data Bank (PDB).[30] As shown in Figure 6A, magenta surface and ribbon represent the Spike RBD and yellow ribbon corresponds to ACE2. The RBD-ACE2 interaction interface is contacted mainly by the N-terminal helix (residues Ile21-Asn51) of ACE2. Our results suggest that SAP6 (Glu37-Gln42, blue ribbon in Figure 6B) and SAP1 (Thr27-Gln42, blue and green ribbon in Figure 6B) are able to disrupt the RBD-ACE2 interaction in the low millimolar range, indicating the importance of these residues at the N-terminal helix of ACE2 for RBD-ACE2 interaction. Based on the crystal structure solved by Lan et al.[30] and highlighted in the modeling studies,[28] polar residues (Glu37, Asp38, Tyr41, and Gln42) of SAP6 are able to form a network of hydrogen bonds with Thr500, Tyr449, Asn501, and Tyr505 of SARS-CoV-2 Spike RBD (Figure 6C). In particular, the carboxy groups of Glu37, Asp38, and Gln42 and hydroxyl group of Tyr41 of SAP6 interface with Spike cavity surrounded by Gln498, Thr500, Tyr449, Asn501, and Tyr505. Taken together, these structural insights lend support to our identification of SAP1 and SAP6 as peptide disruptors of the Spike RBD-ACE2 interaction.

CONCLUSIONS

In summary, we have developed and screened a panel of rationally designed, small peptide inhibitors and identified peptides that block the interaction of coronavirus Spike proteins with ACE2. Importantly, we have identified two peptides, SAP1 and SAP6, which inhibit SARS-CoV-2 infection—demonstrating the feasibility of targeting Spike−ACE2 interaction interface with peptide-based inhibitors to inhibit virus infection. SAP6, which contains the minimal conserved EDLFYQ sequence, highlights the importance of the N-terminal α1 helix of ACE2 for interaction with Spike protein. Future structure-based rational design studies focused on improved conformational matching between SAPs and SARS-CoV-2 Spike protein will allow for increased binding affinity and potent viral inhibition. Such approaches could include increased noncovalent $\pi-\pi$ interactions between aromatic amino acid residues and the enhancement of peptide α-helicity to increase the stability of the SAPs. Lending support to such approaches, a recent study employed computer-generated scaffolds built around the α1 helix of ACE2 to design *de novo* miniprotein inhibitors of SARS-CoV-2.[43] In summary, our proof-of-principle study that SARS-CoV-2 can be inhibited by small peptides will further allow for the successful development of engineered peptides and peptidomimetic-based compounds for the treatment of COVID-19.

METHODS

Peptide Design and Recombinant Proteins. SAPs were designed using the following published structures: SARS-CoV-2 Spike S1 subunit bound to ACE2 (PDB codes: 7A91−98), SARS-CoV-2 RBD bound to ACE2 (PDB codes: 6M0J and 6VW1), SARS-CoV RBD bound to ACE2 (PDB code: 2AJF), and SARS-CoV S1−S2 subunits bound to ACE2 (PDB codes: 6ACK, 6ACJ, 6ACC, 6ACD, and 6ACG).[19,21,26−31] Sequence and structural comparisons of the SARS-CoV and SARS-CoV-2 binding interfaces with ACE2 were performed using Clustal Omega (EMBL-EBI, England), SWISS-MODEL (Biozentrum, Switzerland), and MUSTER (University of Michigan, USA). Once designed, synthetic SAPs were purchased from Biomatik (95% purity, with TFA removed) either unmodified or with an N-terminal FITC label (FITC-SAP). 1× Phosphate Buffered Saline (PBS) was used as a diluent to reconstitute SAPs. To improve the solubility of SAP1 and SAP2, 1× PBS was supplemented with 10% and 5% aqueous NH_3, respectively. Recombinant His-tagged SARS-CoV-2 Spike RBD (His-S RBD, amino acids Arg319-Phe541) was purchased from RayBiotech.

Affinity Precipitation Assay. Affinity precipitation assays using Ni-NTA beads (GE Healthcare) were performed with His-S RBD and FITC-SAPs using previously described methods.[44] Ni-NTA beads were equilibrated in binding buffer (50 mM Tris pH 7.5, 250 mM NaCl, 50 mM imidazole, and 2 mM β-mercaptoethanol). Binding reactions were setup by incubating equilibrated Ni-NTA beads with His-S RBD (1 μM) and increasing concentrations (3, 1, 0.5, 0.25, and 0.125 mM) of indicated FITC-SAP in the binding buffer and incubated for 1 h at 4 °C. In parallel, control reactions with 3 mM of indicated FITC-SAP without His-S RBD were preformed to rule out nonspecific FITC-SAP binding to the Ni-NTA beads. Reactions were spun and washed three times in the binding buffer to remove unbound proteins/peptides. The resulting protein−peptide complexes bound to the beads were extracted using NuPAGE lithium dodecyl sulfate sample buffer (Invitrogen), subjected to SDS-PAGE analysis, and visualized by Coomassie staining or fluorescence detection at 488 nm. Resulting FITC-labeled bands were quantified using ImageJ software. To estimate K_d values for FITC-SAP binding to His-S RBD, the data were fit to the Hill equation using Origin 8 software (OriginLab).

Cells, Plasmids, Viruses. HEK293T (ATCC CRL-3216), HEK293T-ACE2 (BEI Resources), Vero E6 (ATCC CRL-1586), and LLC-MK2 (ATCC CCL-7) cells were cultured in Dulbecco's modified Eagle's medium (DMEM, Gibco) supplemented with 10% fetal bovine serum (FBS, Gibco). HEK293T cells stably expressing GFP-tagged human ACE2 (HEK293T-ACE2-GFP) were generated using methods described previously,[45] and were maintained in DMEM supplemented with 10% FBS and 1 μg/mL puromycin (Sigma).

Plasmid encoding SARS-CoV-2 Spike (pCAGGS-SARS-CoV-2 Spike) was obtained from BEI Resources. Generation of plasmid encoding SARS-CoV Spike (pCAGGS-SARS-CoV Spike) has been described previously.[46] Vesicular stomatitis virus-G (VSV-G) expression plasmid (pMD2.G) was purchased from Addgene. HIV-1-derived luciferase reporter vector (pNL4−3.Luc.R$^-$E$^-$) was obtained from NIH AIDS Reagent Program.

SARS-CoV-2 USA-WA1/2020 stock virus was obtained from BEI Resources. Human coronavirus NL63 (HCoV-NL63) stock was obtained from Dr. Susan Baker (Loyola University, Chicago, IL).

Pseudovirus Production. *Luciferase*-encoding lentiviruses pseudotyped with viral glycoprotein of interest were generated using methods described previously.[47] Briefly, HEK293T cells were transfected with pNL4−3.Luc.R$^-$E$^-$ and pCAGGS-SARS-CoV-2 Spike, pCAGGS-SARS-CoV Spike, or pMD2.G using

https://dx.doi.org/10.1021/acs.bioconjchem.0c00664
Bioconjugate Chem. XXXX, XXX, XXX−XXX

Fugene 6 transfection reagent (Roche) following manufacturer's protocol. Forty-eight hours post-transfection, virus-containing supernatants were harvested, filtered through 0.45 μm sterile filter, and concentrated using Amicon Ultra-15 centrifugal filters (Millipore). Aliquots of pseudoviruses were stored at −80 °C. The titers of SARS-CoV-2 Spike-, SARS-CoV Spike-, and VSV-G-pseudotyped viruses were in the range of ∼2 × 10^5, ∼1 × 10^5, and ∼3 × 10^7 relative luciferase units (RLUs)/mL, respectively.

Pseudovirus Inhibition Assay. HEK293T-ACE2 cells were seeded in μClear Black 96-well plates (Greiner Bio-One) in 100 μL of DMEM supplemented with 10% FBS at a density of 1.25 × 10^4 cells per well. Sixteen hours after plating, equal amounts (RLUs/mL) of a given pseudovirus were incubated with indicated concentrations of the test peptide or diluent control (1× PBS) in 50 μL of DMEM supplemented with 10% FBS for 1 h at 37 °C in a V-bottom 96-well plate. The virus−peptide mixture was then added to the HEK293T-ACE2 cells. Polybrene (Sigma) at the final concentration of 5 μg/mL was added to the cells. After 48 h, 100 μL of supernatant was removed from each well and luciferase activity was measured using Bright-Glo Luciferase Assay System (Promega) following the manufacturer's protocol. Luminescence was detected using an Infinite M PLEX multimode plate reader (Tecan).

Dose Response Curves. For dose response curves, the pseudovirus inhibition assays were performed with increasing concentrations of SAP (0.001, 0.01, 0.1, 1.0, 2.5, 5.0, and 7.5 mM). Percent viral inhibition was calculated as the percent reduction in luciferase activity of pseudovirus incubated with a given concentration of SAP compared to the pseudovirus incubated with the diluent control. The concentration of SAP that resulted in 50% inhibition of viral replication (IC_{50}) was interpolated from a nonlinear, best-fit curve using GraphPad Prism 8.0.2 software.

Biosafety Procedures for Live SARS-CoV-2 Experiments. All experiments involving live SARS-CoV-2 were performed at Biosafety Level 3 (BSL3) according to the standard operating procedures approved by The Ohio State University BSL3 Operations Group (BOG) and Institutional Biosafety Committee. Infected cells were removed from the BSL3 facility for subsequent analyses after fixation with 4% paraformaldehyde for a minimum of 1 h in accordance with a validated decontamination protocol approved by the BOG and Institutional Biosafety Officer.

SARS-CoV-2 Propagation. SARS-CoV-2 USA-WA1/2020 stock was diluted 1:10,000 in DMEM and added to confluent Vero E6 cells. After infection for 1 h at 37 °C, media was replaced with DMEM supplemented with 4% FBS. Following incubation at 37 °C for 72 h, virus-containing supernatant was clarified at 1000*g* for 10 min to remove cell debris, aliquoted, flash-frozen in liquid nitrogen, and stored at −80 °C. The viral stock titer was determined by plaque assay on Vero E6 cells in 12-well plates with 0.3% low-melting agarose (Sigma) overlay and visualization with 0.25% crystal violet (Sigma).

SARS-CoV-2 Infections. 10^6 plaque-forming units of SARS-CoV-2 were incubated with 3 mM final concentration of the test peptide or diluent control (1× PBS) in 400 μL of DMEM for 1 h at 37 °C. The virus−peptide mixture was then added to near-confluent HEK293T-ACE2-GFP cells in a 12-well plate. Infection was allowed to proceed for 1 h at 37 °C at which point media was removed and replaced with 500 μL of DMEM supplemented with 10% FBS. After 24 h, the cells were harvested using 0.25% trypsin-EDTA (Gibco), fixed with 4% paraformaldehyde (Thermo Scientific) for 1 h at room temperature, permeabilized with 1× PBS containing 0.1% Triton X-100, and blocked with 1× PBS containing 2% FBS. The cells were then stained with anti-SARS-CoV-2 N mouse monoclonal antibody (1:1000, Sino Biological) followed by staining with anti-mouse AlexaFluor-647 secondary antibody (1:1000, Life Technologies). The stained cells were analyzed using a FACSCanto II flow cytometer (BD Biosciences). Flow cytometry data was analyzed using FlowJo software.

HCoV-NL63 Propagation. HCoV-NL63 stock was expanded and titered on LLC-MK2 cells as described previously.[48] The virus was aliquoted and stored at −80 °C.

HCoV-NL63 Infections. HCoV-NL63 equiv to MOI of 0.5 was incubated with 3 mM final concentration of the test peptide or diluent control (1× PBS) in 300 μL of DMEM for 1 h at 37 °C. Confluent LLC-MK2 cells in 6-well plates were washed once with DMEM. The virus−peptide mixture was then added to LLC-MK2 cells in triplicate. Infection was allowed to proceed for 1 h at 37 °C at which point media was removed and replaced with 1 mL of DMEM supplemented with 2% FBS. After 72 h, the cytopathic effects (CPE) in each well were imaged under a light microscope. The cell culture supernatants were collected for virus titration by plaque assay.

HCoV-NL63 Plaque Assay. Confluent LLC-MK2 cells in 6-well plates were infected with serial dilutions (ranging from 10^{-1} to 10^{-7}) of HCoV-NL63 in DMEM. After infection for 1 h at 37 °C, cells were washed three times with DMEM and overlaid with 1% low-melting agarose in 2 mL of DMEM supplemented with 2% FBS. After incubation at 37 °C for 5 days, cells were fixed with 4% paraformaldehyde for 2 h, and plaques were visualized after staining with 0.05% crystal violet.

AUTHOR INFORMATION

Corresponding Authors

Amit Sharma − *Department of Microbial Infection & Immunity and Department of Veterinary Biosciences, The Ohio State University, Columbus, Ohio 43210, United States*; orcid.org/0000-0002-3836-5617; Email: sharma.157@osu.edu

Ross C. Larue − *Division of Pharmaceutics and Pharmacology, The Ohio State University, Columbus, Ohio 43210, United States*; Email: larue.22@osu.edu

Authors

Enming Xing − *Division of Medicinal Chemistry and Pharmacognosy, The Ohio State University, Columbus, Ohio 43210, United States*

Adam D. Kenney − *Department of Microbial Infection & Immunity, The Ohio State University, Columbus, Ohio 43210, United States*

Yuexiu Zhang − *Department of Veterinary Biosciences, The Ohio State University, Columbus, Ohio 43210, United States*

Jasmine A. Tuazon − *Medical Scientist Training Program, The Ohio State University, Columbus, Ohio 43210, United States*

Jianrong Li − *Department of Veterinary Biosciences, The Ohio State University, Columbus, Ohio 43210, United States*

Jacob S. Yount − *Department of Microbial Infection & Immunity, The Ohio State University, Columbus, Ohio 43210, United States*

Pui-Kai Li − *Division of Medicinal Chemistry and Pharmacognosy, The Ohio State University, Columbus, Ohio 43210, United States*

https://dx.doi.org/10.1021/acs.bioconjchem.0c00664
Bioconjugate Chem. XXXX, XXX, XXX−XXX

Complete contact information is available at:
https://pubs.acs.org/10.1021/acs.bioconjchem.0c00664

Author Contributions

Conceptualization: R.C.L. and A.S.; research design: R.C.L., E.X., J.L., J.S.Y., P−K.L., A.S.; investigation: R.C.L., E.X., A.D.K., Y.Z., J.A.T., J.S.Y., A.S.; writing—original draft: R.C.L. and A.S.; writing—review and editing: all authors.

Notes

The authors declare the following competing financial interest(s): Ross C Larue and Amit Sharma have filed a provisional patent application for these inhibitors.

■ ACKNOWLEDGMENTS

This research was supported by The Ohio State University's institutional start-up funds to R.C.L. and A.S. We thank Geraldine Vilmen and Natalie Cyberski for technical assistance and helpful discussions. The ToC graphic was created with BioRender.com.

■ REFERENCES

(1) Zhou, P., Yang, X. L., Wang, X. G., Hu, B., Zhang, L., Zhang, W., Si, H. R., Zhu, Y., Li, B., Huang, C. L., et al. (2020) A pneumonia outbreak associated with a new coronavirus of probable bat origin. *Nature 579*, 270−273.

(2) Wu, F., Zhao, S., Yu, B., Chen, Y. M., Wang, W., Song, Z. G., Hu, Y., Tao, Z. W., Tian, J. H., Pei, Y. Y., et al. (2020) A new coronavirus associated with human respiratory disease in China. *Nature 579*, 265−269.

(3) Sanche, S., Lin, Y. T., Xu, C., Romero-Severson, E., Hengartner, N., and Ke, R. (2020) High Contagiousness and Rapid Spread of Severe Acute Respiratory Syndrome Coronavirus 2. *Emerging Infect. Dis. 26*, 1470−1477.

(4) Anfinrud, P., Stadnytskyi, V., Bax, C. E., and Bax, A. (2020) Visualizing Speech-Generated Oral Fluid Droplets with Laser Light Scattering. *N. Engl. J. Med. 382*, 2061−2063.

(5) van Doremalen, N., Bushmaker, T., Morris, D. H., Holbrook, M. G., Gamble, A., Williamson, B. N., Tamin, A., Harcourt, J. L., Thornburg, N. J., Gerber, S. I., et al. (2020) Aerosol and Surface Stability of SARS-CoV-2 as Compared with SARS-CoV-1. *N. Engl. J. Med. 382*, 1564−1567.

(6) Huang, C., Wang, Y., Li, X., Ren, L., Zhao, J., Hu, Y., Zhang, L., Fan, G., Xu, J., Gu, X., et al. (2020) Clinical features of patients infected with 2019 novel coronavirus in Wuhan, China. *Lancet 395*, 497−506.

(7) Wang, D., Hu, B., Hu, C., Zhu, F., Liu, X., Zhang, J., Wang, B., Xiang, H., Cheng, Z., Xiong, Y., et al. (2020) Clinical Characteristics of 138 Hospitalized Patients With 2019 Novel Coronavirus-Infected Pneumonia in Wuhan, China. *JAMA 323*, 1061−1069.

(8) Mao, R., Qiu, Y., He, J. S., Tan, J. Y., Li, X. H., Liang, J., Shen, J., Zhu, L. R., Chen, Y., Iacucci, M., et al. (2020) Manifestations and prognosis of gastrointestinal and liver involvement in patients with COVID-19: a systematic review and meta-analysis. *Lancet Gastroenterol Hepatol 5*, 667−678.

(9) Pezzini, A., and Padovani, A. (2020) Lifting the mask on neurological manifestations of COVID-19. *Nat. Rev. Neurol. 16*, 636−644.

(10) Fernandes, A. C. L., Vale, A. J. M., Guzen, F. P., Pinheiro, F. I., Cobucci, R. N., and de Azevedo, E. P. (2020) Therapeutic Options Against the New Coronavirus: Updated Clinical and Laboratory Evidences. *Front. Med. 7*, 546.

(11) Berlin, D. A., Gulick, R. M., and Martinez, F. J. (2020) Severe Covid-19. *N. Engl. J. Med.*, DOI: 10.1056/NEJMcp2009575.

(12) Cui, J., Li, F., and Shi, Z. L. (2019) Origin and evolution of pathogenic coronaviruses. *Nat. Rev. Microbiol. 17*, 181−192.

(13) Lu, R., Zhao, X., Li, J., Niu, P., Yang, B., Wu, H., Wang, W., Song, H., Huang, B., Zhu, N., et al. (2020) Genomic characterisation and epidemiology of 2019 novel coronavirus: implications for virus origins and receptor binding. *Lancet 395*, 565−574.

(14) Wrapp, D., Wang, N., Corbett, K. S., Goldsmith, J. A., Hsieh, C. L., Abiona, O., Graham, B. S., and McLellan, J. S. (2020) Cryo-EM structure of the 2019-nCoV spike in the prefusion conformation. *Science 367*, 1260−1263.

(15) Belouzard, S., Chu, V. C., and Whittaker, G. R. (2009) Activation of the SARS coronavirus spike protein via sequential proteolytic cleavage at two distinct sites. *Proc. Natl. Acad. Sci. U. S. A. 106*, 5871−5876.

(16) Simmons, G., Reeves, J. D., Rennekamp, A. J., Amberg, S. M., Piefer, A. J., and Bates, P. (2004) Characterization of severe acute respiratory syndrome-associated coronavirus (SARS-CoV) spike glycoprotein-mediated viral entry. *Proc. Natl. Acad. Sci. U. S. A. 101*, 4240−4245.

(17) Shang, J., Wan, Y., Luo, C., Ye, G., Geng, Q., Auerbach, A., and Li, F. (2020) Cell entry mechanisms of SARS-CoV-2. *Proc. Natl. Acad. Sci. U. S. A. 117*, 11727−11734.

(18) Hoffmann, M., Kleine-Weber, H., Schroeder, S., Kruger, N., Herrler, T., Erichsen, S., Schiergens, T. S., Herrler, G., Wu, N. H., Nitsche, A., et al. (2020) SARS-CoV-2 Cell Entry Depends on ACE2 and TMPRSS2 and Is Blocked by a Clinically Proven Protease Inhibitor. *Cell 181*, 271−280.

(19) Li, F., Li, W., Farzan, M., and Harrison, S. C. (2005) Structure of SARS coronavirus spike receptor-binding domain complexed with receptor. *Science 309*, 1864−1868.

(20) Gui, M., Song, W., Zhou, H., Xu, J., Chen, S., Xiang, Y., and Wang, X. (2017) Cryo-electron microscopy structures of the SARS-CoV spike glycoprotein reveal a prerequisite conformational state for receptor binding. *Cell Res. 27*, 119−129.

(21) Benton, D. J., Wrobel, A. G., Xu, P., Roustan, C., Martin, S. R., Rosenthal, P. B., Skehel, J. J., and Gamblin, S. J. (2020) Receptor binding and priming of the spike protein of SARS-CoV-2 for membrane fusion. *Nature 588*, 327.

(22) Letko, M., Marzi, A., and Munster, V. (2020) Functional assessment of cell entry and receptor usage for SARS-CoV-2 and other lineage B betacoronaviruses. *Nat. Microbiol 5*, 562−569.

(23) Simmons, G., Zmora, P., Gierer, S., Heurich, A., and Pohlmann, S. (2013) Proteolytic activation of the SARS-coronavirus spike protein: cutting enzymes at the cutting edge of antiviral research. *Antiviral Res. 100*, 605−614.

(24) Millet, J. K., and Whittaker, G. R. (2015) Host cell proteases: Critical determinants of coronavirus tropism and pathogenesis. *Virus Res. 202*, 120−134.

(25) Madu, I. G., Roth, S. L., Belouzard, S., and Whittaker, G. R. (2009) Characterization of a highly conserved domain within the severe acute respiratory syndrome coronavirus spike protein S2 domain with characteristics of a viral fusion peptide. *J. Virol. 83*, 7411−7421.

(26) Song, W., Gui, M., Wang, X., and Xiang, Y. (2018) Cryo-EM structure of the SARS coronavirus spike glycoprotein in complex with its host cell receptor ACE2. *PLoS Pathog. 14*, e1007236.

(27) Walls, A. C., Park, Y. J., Tortorici, M. A., Wall, A., McGuire, A. T., and Veesler, D. (2020) Structure, Function, and Antigenicity of the SARS-CoV-2 Spike Glycoprotein. *Cell 181*, 281−292.

(28) Wang, Y., Liu, M., and Gao, J. (2020) Enhanced receptor binding of SARS-CoV-2 through networks of hydrogen-bonding and hydrophobic interactions. *Proc. Natl. Acad. Sci. U. S. A. 117*, 13967−13974.

(29) Yan, R., Zhang, Y., Li, Y., Xia, L., Guo, Y., and Zhou, Q. (2020) Structural basis for the recognition of SARS-CoV-2 by full-length human ACE2. *Science 367*, 1444−1448.

(30) Lan, J., Ge, J., Yu, J., Shan, S., Zhou, H., Fan, S., Zhang, Q., Shi, X., Wang, Q., Zhang, L., et al. (2020) Structure of the SARS-CoV-2 spike receptor-binding domain bound to the ACE2 receptor. *Nature 581*, 215−220.

(31) Shang, J., Ye, G., Shi, K., Wan, Y., Luo, C., Aihara, H., Geng, Q., Auerbach, A., and Li, F. (2020) Structural basis of receptor recognition by SARS-CoV-2. *Nature 581*, 221−224.

(32) Barh, D., Tiwari, S., Silva Andrade, B., Giovanetti, M., Almeida Costa, E., Kumavath, R., Ghosh, P., Goes-Neto, A., Carlos Junior Alcantara, L., and Azevedo, V. (2020) Potential chimeric peptides to block the SARS-CoV-2 spike receptor-binding domain. *F1000Research 9*, 576.
(33) Baig, M. S., Alagumuthu, M., Rajpoot, S., and Saqib, U. (2020) Identification of a Potential Peptide Inhibitor of SARS-CoV-2 Targeting its Entry into the Host Cells. *Drugs R&D 20*, 161−169.
(34) Huang, X., Pearce, R., and Zhang, Y. (2020) De novo design of protein peptides to block association of the SARS-CoV-2 spike protein with human ACE2. *Aging 12*, 11263−11276.
(35) Han, Y., and Kral, P. (2020) Computational Design of ACE2-Based Peptide Inhibitors of SARS-CoV-2. *ACS Nano 14*, 5143−5147.
(36) Millet, J. K., Tang, T., Nathan, L., Jaimes, J. A., Hsu, H. L., Daniel, S., and Whittaker, G. R. (2019) Production of Pseudotyped Particles to Study Highly Pathogenic Coronaviruses in a Biosafety Level 2 Setting. *J. Visualized Exp.*, e59010.
(37) Finkelshtein, D., Werman, A., Novick, D., Barak, S., and Rubinstein, M. (2013) LDL receptor and its family members serve as the cellular receptors for vesicular stomatitis virus. *Proc. Natl. Acad. Sci. U. S. A. 110*, 7306−7311.
(38) Wang, Y., Grunewald, M., and Perlman, S. (2020) Coronaviruses: An Updated Overview of Their Replication and Pathogenesis. *Methods Mol. Biol. 2203*, 1−29.
(39) Pyrc, K., Berkhout, B., and van der Hoek, L. (2007) Identification of new human coronaviruses. *Expert Rev. Anti-Infect. Ther. 5*, 245−253.
(40) Baker, S. C. (2004) Coronaviruses: from common colds to severe acute respiratory syndrome. *Pediatr Infect Dis J. 23*, 1049−1050.
(41) Hofmann, H., Pyrc, K., van der Hoek, L., Geier, M., Berkhout, B., and Pohlmann, S. (2005) Human coronavirus NL63 employs the severe acute respiratory syndrome coronavirus receptor for cellular entry. *Proc. Natl. Acad. Sci. U. S. A. 102*, 7988−7993.
(42) Wu, K., Li, W., Peng, G., and Li, F. (2009) Crystal structure of NL63 respiratory coronavirus receptor-binding domain complexed with its human receptor. *Proc. Natl. Acad. Sci. U. S. A. 106*, 19970−19974.
(43) Cao, L., Goreshnik, I., Coventry, B., Case, J. B., Miller, L., Kozodoy, L., Chen, R. E., Carter, L., Walls, A. C., Park, Y. J., et al. (2020) De novo design of picomolar SARS-CoV-2 miniprotein inhibitors. *Science 370*, 426−431.
(44) Larue, R. C., Plumb, M. R., Crowe, B. L., Shkriabai, N., Sharma, A., DiFiore, J., Malani, N., Aiyer, S. S., Roth, M. J., Bushman, F. D., et al. (2014) Bimodal high-affinity association of Brd4 with murine leukemia virus integrase and mononucleosomes. *Nucleic Acids Res. 42*, 4868−4881.
(45) McMichael, T. M., Zhang, Y., Kenney, A. D., Zhang, L., Zani, A., Lu, M., Chemudupati, M., Li, J., and Yount, J. S. (2018) IFITM3 Restricts Human Metapneumovirus Infection. *J. Infect. Dis. 218*, 1582−1591.
(46) Hofmann, H., Hattermann, K., Marzi, A., Gramberg, T., Geier, M., Krumbiegel, M., Kuate, S., Uberla, K., Niedrig, M., and Pohlmann, S. (2004) S protein of severe acute respiratory syndrome-associated coronavirus mediates entry into hepatoma cell lines and is targeted by neutralizing antibodies in infected patients. *J. Virol. 78*, 6134−6142.
(47) Nahabedian, J., Sharma, A., Kaczmarek, M. E., Wilkerson, G. K., Sawyer, S. L., and Overbaugh, J. (2017) Owl monkey CCR5 reveals synergism between CD4 and CCR5 in HIV-1 entry. *Virology 512*, 180−186.
(48) Chen, Z., Wang, Y., Ratia, K., Mesecar, A. D., Wilkinson, K. D., and Baker, S. C. (2007) Proteolytic processing and deubiquitinating activity of papain-like proteases of human coronavirus NL63. *J. Virol. 81*, 6007−6018.

https://dx.doi.org/10.1021/acs.bioconjchem.0c00664
Bioconjugate Chem. XXXX, XXX, XXX−XXX